IOP Publishing Journal of Physics: Condensed Matter
J. Phys.: Condens. Matter **32** (2020) 235402 (9pp) https://doi.org/10.1088/1361-648X/ab7031

Ab initio calculations of the crystal field and phonon dispersions in $CePd_2Al_2$ and $LaPd_2Al_2$

D Legut[1,2], M Diviš[3], P Doležal[3], S H Zhang[1,4] and P Javorský[3]

[1] IT4Innovations, VSB-Technical University of Ostrava, 17. listopadu 2172/15, 708 00 Ostrava, Czech Republic
[2] Nanotechnology Centre, VSB-Technical University of Ostrava, 17. listopadu 2172/15, 708 00 Ostrava, Czech Republic
[3] Charles University, Faculty of Mathematics and Physics, Department of Condensed Matter Physics, Ke Karlovu 5, 121 16 Prague 2, Czech Republic
[4] School of Materials Science and Engineering, Beihang University, Beijing 100191, People's Republic of China

E-mail: dominik.legut@vsb.cz

Received 6 September 2019, revised 18 December 2019
Accepted for publication 27 January 2020
Published 12 March 2020

Abstract

$CePd_2Al_2$ crystallizes in the $CaBe_2Ge_2$-type tetragonal structure (*P*4/*nmm*, 129) and undergoes a phase transition to the orthorhombic *Cmme* structure at around 13 K. Its inelastic neutron spectra reveal an additional magnetic excitation that was ascribed to electron-phonon interaction leading to a formation of a new quantum quasi-bound vibron state. We present the first-principles calculations of the crystal field excitations and lattice dynamics calculations of the phonon dispersions to compare with the experimental data. The calculated crystal field energy splitting in $CePd_2Al_2$ agrees well with the model used to describe the experimental neutron scattering spectra. The first excited crystal field level moves to higher energies when undergoing the transformation from tetragonal to orthorhombic structure, in agreement with the experiment. The analysis based on calculated elastic constants and lattice dynamics calculations show that in both tetragonal and orthorhombic structures there are no imaginary modes for any q-wave vector within the Brillouin zone, and therefore the lattice structures are stable. The phonon dispersions and density of states are calculated for both crystal structures of $CePd_2Al_2$ and its nonmagnetic counterpart $LaPd_2Al_2$. The results generally agree well with the experimental data including the high phonon density of states around 12 meV. The phonon density of states is also used to calculate the mean squared displacement, Debye temperature, lattice heat capacity and compared with similar properties of the available experiment.

Keywords: phonons, crystal field, heavy fermion, vibron, thermodynamics

(Some figures may appear in colour only in the online journal)

1. Introduction

The tetragonal CeT_2X_2 compounds (where T = transition metal d-element and X = p-metal) form a large group of materials which exhibit various interesting physical properties as heavy-fermion behavior, valence-fluctuations, non-Fermi-liquid behavior, or unconventional superconductivity. [1–5] These interesting properties stem from competition between RKKY and Kondo interactions and a strong influence of crystal field surrounding the Ce ions. The observation of an additional magnetic excitation in the neutron scattering spectra of $CePd_2Al_2$ is another interesting phenomenon. [6, 7] The existence of three excitations from the ground state of Ce^{3+} ions cannot be explained in terms of pure crystal field splitting and was ascribed to electron-phonon interaction leading to a formation of a new quantum quasi-bound vibron

state similar to $CeAl_2$ [8, 9] and $CeCuAl_3$ [10]. This strong magneto-elastic coupling between orbital and lattice degrees of freedom and the resulting magneto-phonon mode have been described within the Thalmeier–Fulde model in the case of cubic $CeAl_2$. [11]

$CePd_2Al_2$ crystallizes in the $CaBe_2Ge_2$-type tetragonal structure (*P*4/*nmm*, 129) and undergoes a phase transition to the orthorhombic *Cmme* structure at around $T_{\text{struc}}^{CePd_2Al_2} = 13$ K [6, 12–14]. Similar structural phase transition is also observed in $LaPd_2Al_2$ [6, 12] excluding a magneto-elastic origin of the phase transition. The structural instability is not unusual in this family of compounds. Phase transition from tetragonal to lower symmetry structures are observed in e.g. $CeNi_2Sn_2$, [15] $CePt_2Sn_2$, [15] $CeRh_2Sb_2$, [16] $CePt_2Ge_2$ [17] or $CePd_2Ga_2$. [18, 19] The magnetic properties of $CePd_2Al_2$ are characterized by an antiferromagnetic order below $T_N = 2.7$ K [13]. The ground state magnetic structure is an amplitude modulated wave described by an incommensurate propagation vector $\vec{k} = (\delta_x, \frac{1}{2} + \delta_y, 0)$ with $\delta_x = 0.06$ and $\delta_y = 0.04$. The magnetic moments order antiferromagnetically within the planes stacked along the *c*-axis and are arranged along the direction close to the orthorhombic *a*-axis [7]. The recent neutron scattering experiment provided a clear link between the observed magnetic excitations and structural properties of $CePd_2Al_2$. The comparison of magnetic excitations measured above and below 13 K, where the structural transition from the tetragonal to the orthorhombic structure occurs, shows a strong shift of the energy of the first excited level to higher energies when cooling below 13 K. [7] The other two excitations are almost unaffected by this transition. These results motivated our *ab initio* calculations of the phonon spectra and crystal field excitations in both structural phases of $CePd_2Al_2$ to explore origin of the experimentally observed changes in energy spectra.

2. Computational details

We performed first-principles electronic structure calculations using the general potential linearised augmented plane wave method (APW + lo, WIEN2k) [20]. The Kohn–Sham equations were solved within the generalized gradient approximation (GGA) [21]. The relativistic effects were treated using scalar relativistic approximation. Atomic sphere radii (AS) of 2.5, 2.1, and 1.8 Bohr radius (1 Bohr radius = 52.9177 pm) were chosen for Ce, Pd, and Al, respectively. About 1400 linearized augmented plane waves (140 per atom) were used in the interstitial region and the highest value of 12 in the expansion of radial wave functions inside the AS to represent the valence states. The correlated Ce 4f states were treated in the open-core approximation and thus are characterized by integer number occupation $4f^1$. We have carefully checked the convergence of the calculation with these parameters. The first principles crystal field (CF) calculations were performed using the method described in [22]. Within this method, the electronic structure and ground states charge density are obtained using the full potential APW + lo method. The CF parameters of the microscopic CF hamiltonian originate from the aspherical part of the total single particle DFT potential in the crystal. To eliminate the self interaction, the self-consistent procedure is first converged with the 4*f* electrons in core [22], which is the open-core approximation used in this work.

To obtain the dynamical properties, the Hellmann–Feynman (HF) forces acting on the atoms starting from the equlibrium are required. In order to do so, we have utilized the unspin-polarized density functional theory method implementing the projector-augmented wave (PAW) formalism [23, 24] to describe the electron-ion interactions as implemented in the VASP code [23, 24]. The approximation for the exchange-correlation potential was used the same as in WIEN2k calculations, i.e. GGA. The Kohn–Sham wave functions are expanded into plane waves up to a cutoff energy of 600 eV. The valence electrons of cerium, lanthanum, palladium, and aluminium atoms are represented by configurations of $5s^25p^65d^16s^2$, $5s^25p^64f^15d^16s^2$, $5s^14d^9$, and $3s^23p^1$, respectively. The calculations for the geometry optimization used the $13 \times 13 \times 8(18 \times 18 \times 8)$ Monkhorst–Pack mesh of **k**-points for the orthorhombic(tetragonal) phase and the convergence criteria for the system's total energy and residual HF forces were of 10^{-7} eV and 10^{-4} eV Å^{-1}, respectively.

The dynamical properties of the both $LaPd_2Al_2$ and $CePd_2Al_2$ lattice are obtained within the quasi-harmonic approximation and the direct method [25, 26] using the Phonopy code [26], which utilizes the DFT calculated HF forces acting on all atoms in a given supercell. Phonons are calculated for the supercells composed of 80 atoms (16 Ce(La), 32 Pd and 32 Al atoms), which are created from the optimized unit cells. Such supercells were found to be large enough to avoid contributions from atoms belonging to the periodic images, as confirmed by the elements of the force constant matrices, which decay by more than three orders of magnitude at the distances smaller than the boundaries of the supercells. The Brillouin zone integration is performed with the reduced number of *k*-points $7 \times 7 \times 3(9 \times 9 \times 3)$ for the tetragonal (orthorhombic) phases. The non-vanishing HF forces required to construct respective dynamical matrix $\mathbf{D}(\mathbf{k})$ are generated by displacing the symmetry non-equivalent Ce(La), Pd, and Al atoms from their equilibrium positions by the amplitude of ± 0.01 Å. Hence, for each configuration the total number of the calculated displacements amounts to 10 for both phases.

The mechanical properties (including elastic constants, elastic moduli, Pugh ratio, and universal anisotropy index) in this work were determined via the AELAS code [36], which was developed as automatic elastic property derivations via high-throughput first-principles computation.

3. Results and discussion

The crystal field parameters and corresponding energy levels have been calculated assuming the two crystal structures of $CePd_2Al_2$—high-temperature tetragonal ($CaBe_2Ge_2$-type) and low-temperature orthorhombic *Cmme*. The structural parameters have been taken from experiment. [7] The results are summarized in table 1 for both tetragonal and orthorhombic

Table 1. The calculated crystal field parameters for tetragonal and orthorhombic phase of $CePd_2Al_2$ in Steven's notation Blm∗Olm [22]. The meV units are used for both Blm and the energy splitting Δ.

	B20	B22	B40	B42	B44	Δ_1	Δ_2
Tetragonal	0.655	0.0	0.109×10^{-2}	0.0	0.173×10^{-1}	3.6	11.8
Orthorhombic	0.628	−0.389	0.104×10^{-2}	-0.405×10^{-2}	-0.127×10^{-1}	4.8	12.2

Table 2. The calculated lattice parameters a, b, c in Å and internal degrees of freedom (z_X, X = Ce/La,Pd,Al). The experimental parameters in brackets are taken from [7] (orthorhombic Ce-phase) and [19] (tetragonal Ce-phase and both La-phases).

$CePd_2Al_2$	a(Å)	b(Å)	c(Å)	z_{Ce}	z_{Pd}	z_{Al}
Tetragonal	4.435(4.415)	—	10.090(9.874)	0.752	0.372	0.123
Orthorhombic	6.274(6.268)	6.271(6.132)	10.089 (9.886)	0.753(0.756)	0.372 (0.371)	0.124(0.119)
$LaPd_2Al_2$	a(Å)	b(Å)	c(Å)	z_{La}	z_{Pd}	z_{Al}
Tetragonal	4.451(4.441)	—	10.087(9.896)	0.753(0.749)	0.371(0.376)	0.121(0.138)
Orthorhombic	6.334(6.313)	6.242(6.195)	10.105 (9.922)	0.752(0.745)	0.371(0.377)	0.129(0.149)

Ce positions in the corresponding crystal structures. Both CF hamiltonians are dominated by second order term B20. This is the reason that the full splitting of the Ce^{3+} ground state multiplet remains similar for both tetragonal and orthorhombic phases. In the tetragonal structure, the second excited state lies at 11.8 meV what perfectly fits to energy of the hypothetical crystal field level assumed around 12 meV when analyzing the neutron scattering data [7]. The energy of this level changes only marginally when going from the tetragonal to the orhorhombic phase. The first excited level is calculated to be at 3.6 meV which is noticeably higher than the experimental value of 1.4 meV. [7] Possible explanation can be the complete neglect of hybridization in our first principles CF calculations. In compounds the hybridization of 4*f* states with valence states is very sensitive to the details of position of the 4*f* levels [27]. This crystal field level then considerably shifts to higher energies when undergoing transition to the orthorhombic phase. This is in a qualitative agreement with the experimental observation [7].

On the other hand, we think that our first principles CF calculations are more suitable than those published recently [29]. We are taking into account two radial nodes for anisotropy of 5d charge density which is very important for the resulting crystal field anisotropy of localized 4f charge density [22]. In the work [29] authors substituted the rare earth ion by yttrium ion. Therefore they are using 4d radial charge density which has one node only.

Prior to the investigation of the lattice dynamics the geometrical optimizations need to be performed for the tetragonal *P*4/*nmm* and orthorhombic *Cmme* phases of $CePd_2Al_2$ and $LaPd_2Al_2$. Lattice parameters as well as the optimized internal degrees of freedom are summarized and compared to the experimental data in table 2. Calculated lattice constants agree well with the recorded ones, being slightly higher, but no more than 2%, than the measured ones. This is a typical feature of the PBE functional for the exchange-correlations effects that tends to underestimate the binding energy. The overall agreement is therefore very good. The relaxed internal degrees of freedom, *z*-component of the Wyckoff positions (for details see [7]) show excellent agreement.

Lattice dynamics was investigated for both $CePd_2Al_2$ and $LaPd_2Al_2$. The dispersion relations of orthorhombic and tetragonal structures along Γ(0, 0, 0) → Z(0.0, 0.0, 0.5) → T(0, 0.5 0.5) → Y(0, 0.5, 0) → S(0.5, 0.5, 0.0) → R(0.5, 0.5, 0.5) and Z(0.0, 0.0, 0.5)→ Γ(0, 0, 0) → M(0.5, 0.5, 0.0) → X(0.0, 0.5, 0.0) → Γ(0, 0, 0) → A(0.5 0.5 0.5) → M(0.5 0.5 0) are shown in figures 1 and 2, respectively. In both structures, there are no imaginary modes for any q-wave vector within the Brillouin zone and therefore the lattice structures are stable. $CePd_2Al_2$ in both structures has higher slopes see, e.g. the ones between the Γ and Z point, i.e. along the (00ζ) direction that indicates higher elastic stiffness along the *c*-axis. Another difference concerns the degeneracy of the transversal modes in the case of the tetragonal structure that is much higher in the case of $LaPd_2Al_2$ with respect to $CePd_2Al_2$, see transversal modes, e.g. along Γ to X and Γ to M, respectively.

The total and partial phonon density of states (DOS), for definition see, e.g. [30], for both $CePd_2Al_2$ and $LaPd_2Al_2$ are depicted in figures 3 and 4, respectively. The total phonon DOS for both compounds is very similar as regard frequency range owing to the fact that the mass difference is also small ($M_{Ce} = 140.115$, $M_{La} = 138.906$). Optical and acoustic frequencies are separated in both compounds and structures by a gap in the frequency range of 18.2–26.9 meV. The low frequency vibrations, in the range of 0–18.2 meV, are dominated by the motions of the rare earth metal as well as palladium. The Al atoms vibrate at much higher frequencies. Here, the shape of the spectra for tetragonal structure is also very similar between both rare earth- based compounds with higher frequencies of $CePd_2Al_2$. In contrast, the orthorhombic structure shows a large shift of phonon DOS at the higher frequencies (Al vibrations) for the Ce- versus $LaPd_2Al_2$ compound. Please note the distinction of the frequency range of vibrations for the Al atoms, i.e. a clear difference between motions of atoms with Wyckoff positions 2*c* and 2*b* and 4*b* and 4*g* of tetragonal and orhorhombic structure, respectively. Also, for the orthorhombic structure the center of mass of the lower frequency of phonon DOS (R + Pd atoms) is shifted by ca 2.1 meV to higher frequencies for $CePd_2Al_2$ with respect to $LaPd_2Al_2$. There is also a remarkable shift of the low frequency

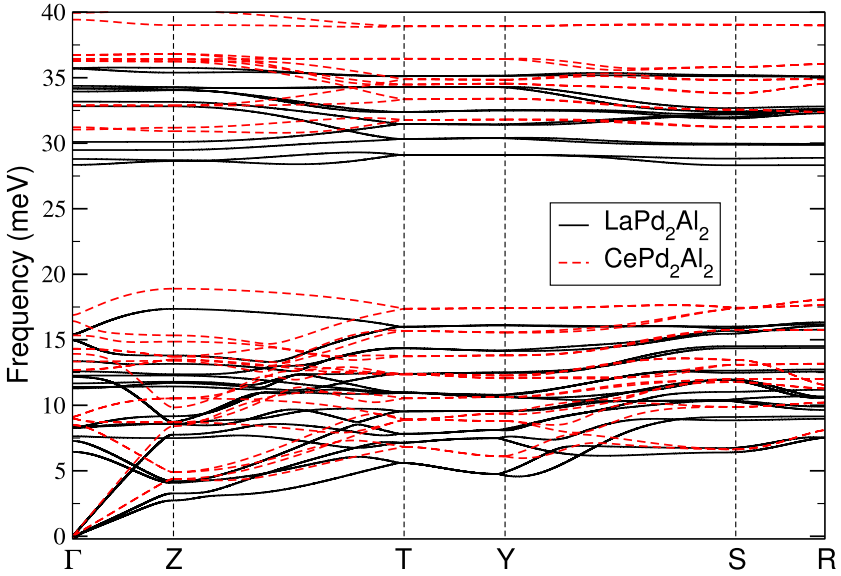

Figure 1. Phonon dispersion relation of $LaPd_2Al_2$ and $CePd_2Al_2$ in orthorhombic structure (*Cmme*, 67).

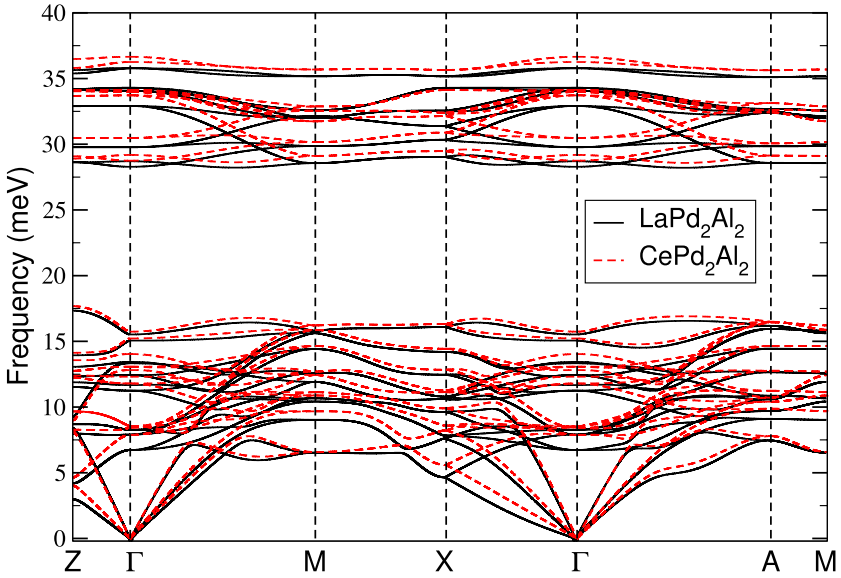

Figure 2. Phonon dispersion relation of $LaPd_2Al_2$ and $CePd_2Al_2$ in tetragonal structure ($P4/mmm$, 129).

DOS (R + Pd atoms) to higher energies in the orthorhombic structure of $CePd_2Al_2$ with respect to the tetragonal one. No such shift occurs for $LaPd_2Al_2$.

The total phonon density of states allows us to estimate the Debye temperature (Θ_D). Using lower frequencies of 0–8.3 meV and fitting function of $\Theta_D(\omega) = a\omega^2$, where a is a parameter for the fitting function of $\Theta_D = (\frac{9N}{a})^{1/3}$, where N is the number of atoms in the unit cell. The total DOS of $LaPd_2Al_2$ in both structures is similar, see figures 3 and 4, and therefore the estimated Debye temperatures are practically the same, $\Theta_D = 185(183)$ K for the orhorhombic(tetragonal) structure, respectively. A slighlty larger difference is in the case of $CePd_2Al_2$, here $\Theta_D = 189$ K versus 205 K between the tetragonal and orthorhombic one. The calculated Debye temperature for $LaPd_2Al_2$ is considerably larger than the one obtained from measurements of specific heat and electric resistivity, ($\Theta_D = 117 - 127$ K [31]), yet in a very good agreement with the value obtained by Kitagawa *et al*, $\Theta_D = 174$ K [18]. In fact, the results of the models used in both references are in agreement considering that the former one considers only the three acoustic branches for the Θ_D evaluation at very low temperatures while Θ_D in the latter one corresponds to the total number of 15 phonon branches. Our calculation is in line with the latter approach.

The calculated phonon DOS enable us to evaluate some thermodynamical quantities that are phonon-dependent. Here, we restrict our investigations to phonons calculated within the harmonic approximation (quasi-harmonic approximation) and analyze the phase stability, mean-squared amplitudes of atomic vibrations (U_{ij}), and the lattice contribution to the

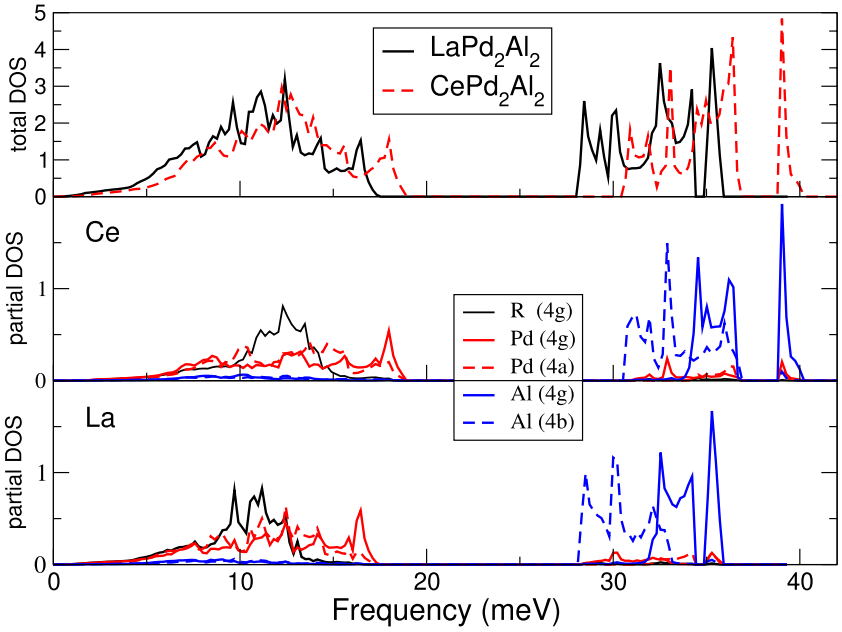

Figure 3. Total and partial density of states in (states/meV) of $LaPd_2Al_2$ and $CePd_2Al_2$ in orthorhombic structure (*Cmme*, 67).

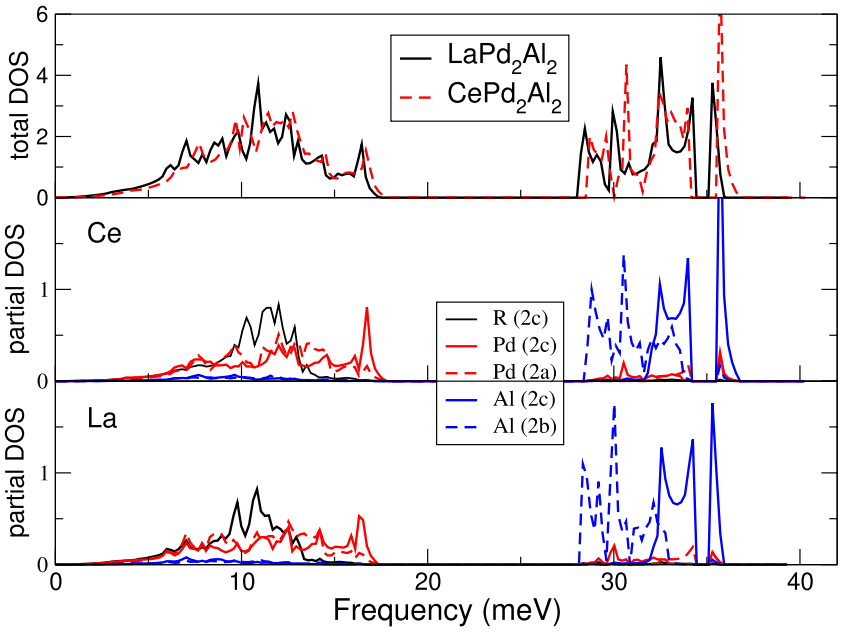

Figure 4. Total and partial density of states in (states/meV) of $LaPd_2Al_2$ and $CePd_2Al_2$ in tetragonal structure ($P4/mmm$, 129).

heat capacity as a function of temperature. The lattice vibrations stabilize the orthorhombic structure with respect to the tetragonal one. Without including phonons the energy difference is 0.75(0.423)meV/f.u. while including motions at T = 0 the differences amount to 11.3(3.4)meV/f.u. for the $CePd_2Al_2$($LaPd_2Al_2$).

Furthermore, to guarantee the positive definiteness of strain energy upon lattice distortion, as formulated by Born [33], the mechanical stability criterion requires the following conditions regardless of the crystal symmetry: positive eigenvalues are required for the matrix of elastic constants. Accordingly, the necessary and sufficient elastic stability conditions are proposed [34] for the tetragonal *P*4/*nmm*: $C_{11} > |C_{12}|$, $2C_{13}^2 < C_{33}(C_{11} + C_{12})$, $C_{44} > 0$, and $C_{66} > 0$; and for the orthorhombic *Cmme*: $C_{11} > 0$, $C_{11}C_{22} > C_{12}^2$, $C_{11}C_{22}C_{33} + 2C_{12}C_{13}C_{23} - C_{11}C_{23}^2 - C_{22}C_{13}^2 - C_{33}C_{12}^2 > 0$, $C_{44} > 0, C_{55} > 0$, and $C_{66} > 0$. The values of the left-hand sides of the stability conditions are summarized in the table 3 and none of them is broken for the tetragonal *P*4/*nmm* and orthorhombic *Cmme* phases of $CePd_2Al_2$ and $LaPd_2Al_2$. Therefore, they are considered to be mechanically stable. The Pugh ratio (i.e. the ratio of the shear to bulk modulus *G*/*B*) was also calculated, which is known as basic parameters to estimate the brittleness or ductility of a materials. Basically, if $G/B < 0.57$ the material is more ductile, otherwise the materials behave in a brittle manner [37]. Therefore, it is found that

Table 3. Elastic constants (C_{ij}), shear modulus (G), bulk modulus (B), Pugh ratio (G/B), and universal anisotropy index (A^U) obtained using the Hill approximation [35] in GPa for the tetragonal $P4/nmm$ and orthorhombic $Cmme$ phases of $CePd_2Al_2$ and $LaPd_2Al_2$.

	C_{11}	C_{12}	C_{13}	C_{22}	C_{23}	C_{33}	C_{44}	C_{55}	C_{66}	G	B	G/B	A^U
Tetragonal $CePd_2Al_2$	145.5	62.0	86.8	—	—	131.2	30.0	—	6.9	21.7	99.2	0.2	2.4
Orthorhombic $CePd_2Al_2$	140.3	92.5	98.0	125.2	92.4	140.2	30.4	35.3	30.6	26.7	107.5	0.25	0.3
Tetragonal $LaPd_2Al_2$	131.8	62.4	86.2	—	—	125.1	22.1	—	3.8	15.5	95.0	0.2	3.9
Orthorhombic $LaPd_2Al_2$	92.6	84.9	93.4	123.4	86.3	99.9	21.3	36.7	26.5	12.9	92.5	0.14	13.4

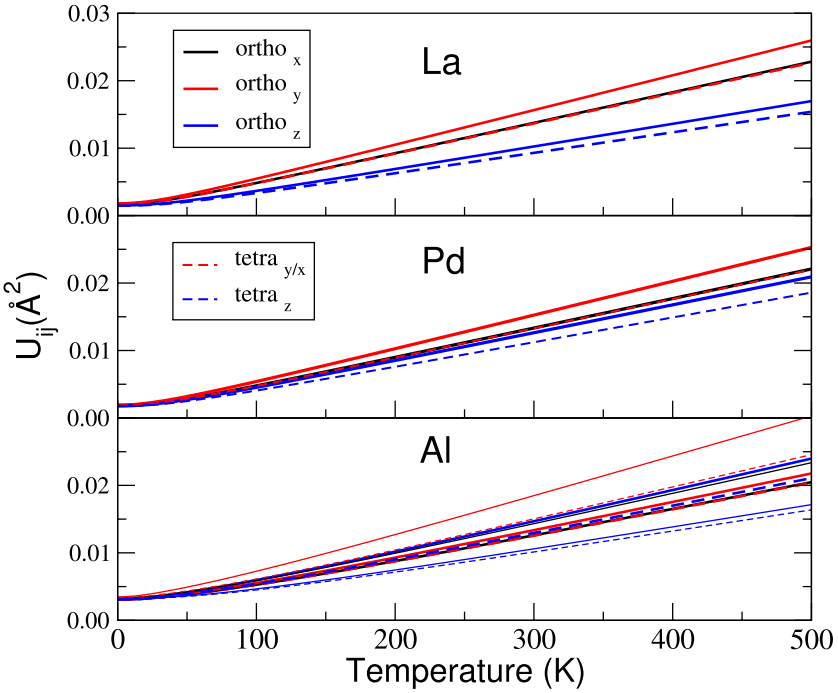

Figure 5. Mean square displacements (MSD) of the $LaPd_2Al_2$. The solid and dashed line mark for the orthorhombic and tetragonal structure, respectively.

Table 4. On-site force constants Φ_{ij} of La($4g$), Pd($4g, 4a$), and Al($4g, 4b$) atoms in the $LaPd_2Al_2$ crystal. The force constants are given in (N/m).

Atom	Φ_{11}	Φ_{22}	Φ_{33}
La(4g)	3.8	3.6	4.8
Pd(4g)	5.5	5.7	7.2
Pd(4a)	5.7	5.5	4.6
Al(4g)	6.6	6.5	7.1
Al(4b)	5.5	5.6	5.2

all of the tetragonal *P*4/*nmm* and orthorhombic *Cmme* phases of $CePd_2Al_2$ and $LaPd_2Al_2$ behave in a ductile manner, and $LaPd_2Al_2$ is more ductile than $CePd_2Al_2$ as a lower value of G/B. And as shown in table 3, orthorhombic $LaPd_2Al_2$ shows a much higher elastic anisotropy with the largest value (13.36) of A^U, while orthorhombic $CePd_2Al_2$ has a much lower value (0.28) of A^U, indicating it is nearly isotropic.

Mean-squared vibrational amplitudes of a given atom in crystal lattice constitute a second-rank symmetric tensor, and they can be expressed by the diagonal and off-diagonal partial phonon DOS [30, 32]. In figure 5 the U_{ij} in $Å^2$ is displayed for the $LaPd_2Al_2$.

Due to the site symmetries of particular atoms in tetragonal and orthorhombic structure one can see that the former has two independent components, for the latter three. In addition, MSD for the Pd atoms ($2a, 2c$) for tetragonal and for orthorhombic ($4g, 4a$) structures are very similar, with only one of them being shown in figure 5 for clarity. In the case of Al atoms, they differ for both structures, which indeed is in accord with respect to the larger differences at which frequencies the Al atoms ($2c, 2b$) and ($4g, 4b$) vibrate, see

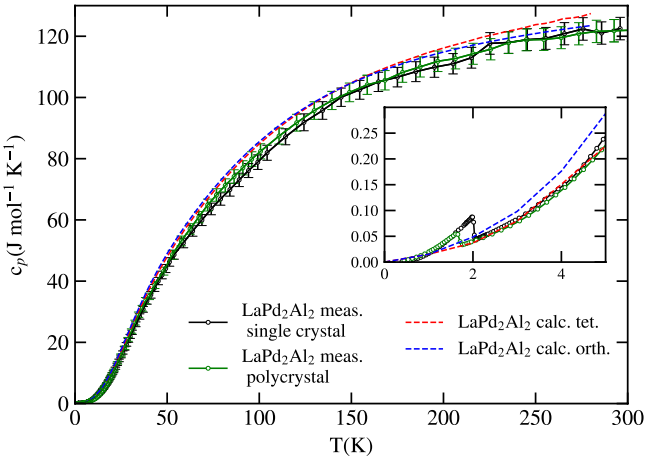

Figure 6. Comparison of measured and calculated specific heat of $LaPd_2Al_2$. The calculated curve includes, beside the dominant phonon contribution, also the electronic part taking the experimentally determined gamma coefficient of 15 $mJmol^{-1}\ K^{-2}$ from [31]. Indicated error bars correspond to about three percent of the measured values.

corresponding partial phonon DOS in figures 4 and 3, respectively. The Al with higher(lower) frequencies are marked by thick(thin) lines in lower panel of figure 5. All mean-squared displacements exhibit typical increase with temperature due to applied harmonic approximation. Here, one can identify that for the La atom the U_{22} (ortho-y in figure 5) shows the highest vibration amplitude, higher than along the *a*-axis despite having the same lattice vectors, see table 2. The U_{33} is lower by 50% indicating much lower thermal motion along the *c*-axis. Similarly for the Pd atoms where now only small difference in the MSD U_{11} and U_{33}, i.e. between the motions

along x-axis and c-axis for the orthorhombic structure was determined being lower than the vibration along the b-axis. Again, the $U_{22} = U_{11} > U_{33}$ of the tetragonal structure is rigidly shifted to lower values with respect to orthorhombic structure. An indications for more rigid tetragonal structure is seen from the slightly higher slopes of the frequencies along the $\Gamma \rightarrow Z$ dispersions in figures 1 and 2. Interesting situation appears for the Al atoms. The ones with higher phonon frequencies (i.e. at $4g$) have U_{22} and U_{33} about 1/3 lower than the other Al atom (at Wyckoff position $4b$). The former Al atom vibrates almost isotropically ($U_{11} \approx U_{22} \approx U_{33}$). This is even more pronounced for the tetragonal structure, see lower panel of figure 5. Let us note that here also for Al in $4g(2c)$ in orthorhombic(tetragonal) structure has $U_{33} > U_{22}$.

Such strong distinction in MSD between the Al atoms is a surprise, to some extent, assuming the same Al mass, but in accord with the calculated partial phonon DOS, (figures 3 and 4), where basically both Al atoms at inequivalent crystal positions vibrate at almost distinct frequency ranges. It is also reflected by the difference in the on-site force constants Φ_{33} versus Φ_{11} and Φ_{22}, see table 4 for all on-site (Φ_{ij}) of all atoms for the $LaPd_2Al_2$ in the orthogonal structure. Here, the Φ_{33} is slightly higher (lower) than Φ_{11}, Φ_{22} for the Al in $4g(4b)$ position. Therefore, the difference of the MSD behavior among the Al atoms is related to the larger stiffness of Al in $4b$ position (lower Φ_{ij}) allowing even less thermal motion along the c-axis.

The quasiharmonic approximations, i.e. harmonic approximations for a number of volumes, allow us to evaluate the thermodynamical functions as volume-dependent (i.e. at constant pressure). This is indeed more desirable as such situation is often found for many experimental measurements rather than studies at a constant volume. If the minimum of the Gibbs energy is found for every temperature and pressure(volume)

$$G(T,p) = \min V[F(T,V) + pV]$$

where Helmholtz free energy $F(T,V)$ consists of internal energy $U(V)$ and phonon free energy F_{ph}(T,V) then properties such as volumetric thermal expansion coefficient β and heat capacity at constant pressure C_p are obtained from the calculated equilibrium volumes $V(T)$ at dense temperature points T:

$$\beta(T) = \frac{1}{V(T)} \frac{\partial V(T)}{\partial T}$$

$$C_p(T,p) = -T\frac{\partial^2 G(T,p)}{\partial T^2} = C_V(T,V(T,p)) + T\frac{\partial V(T,p)}{\partial T}\left.\frac{\partial S(T,V)}{\partial V}\right|_{V=V(T,p)}$$

where the second term of the last equation is the contribution to heat capacity from thermal expansion [26] and the C_V is computed as

$$C_V = \left(\frac{\partial E}{\partial T}\right) = \sum_{\vec{q}m} C_{\vec{q}m} = \sum_{\vec{q}m} k_B \left(\frac{\hbar\omega_{\vec{q}m}}{k_B T}\right)^2 \frac{e^{(\hbar\omega_{\vec{q}m})/(k_B T)}}{[e^{(\hbar\omega_{\vec{q}m})/(k_B T)} - 1]^2}. \quad (1)$$

From the equation it follows that C_V and C_P are related as

$$C_p = C_v + TV\beta^2/B.$$

For more details, see e.g. [28]. In our study, the experimental measurements were done at constant pressure and hence the calculated C_p is compared with the recorded data in figure 6 for $LaPd_2Al_2$. The specific heat of $LaPd_2Al_2$ is reproduced with a reasonably good agreement. Rather surprisingly, the calculation corresponding to the tetragonal lattice agrees almost perfectly with the experimental data while the data for the orthorhombic structure slightly exceed the measured values in the low-temperature part (just above the T_c). The discrepancy between the theoretical and experimental values of C_p at higher temperatures is comparable with usual experimental uncertainty. The absolute value of the experimental error of the heat capacity increases with increasing temperature due to various reasons. We added error bars in figure 6 considering usual 3 percent error at higher temperatures to document this experimental uncertainty. We remind that $LaPd_2Al_2$ undergoes the structural transition to the orthorhombic phase around 90 K. [6, 12, 19], so we would expect better agreement with the orthorhombic lattice calculation at low temperatures. The direct comparison for $CePd_2Al_2$ is not possible because the specific heat of the Ce material includes also significant magnetic contribution and large heat capacity connected with the structural phase transition at 13 K.

Let us finally relate all the calculated results to the inelastic neutron scattering data [7] being it the primary goal of this work. The simultaneous occurrence of high density of phonon states and the CF level at the same energy is the key prerequisite for the magnetoelastic coupling and formation of the vibron states. Our present calculations are fully in agreement with such a scheme. The high phonon density of states around 12 meV is (i) in good agreement with the experimental observation [7] and (ii) appears at energy which is the same or very close to the calculated energy of the second CF excited state. It should be noted that there is no CF excitation experimentally observed around 12 meV, but it is just the energy of the hypothetical CF level assumed when analyzing the neutron scattering data [7].

When undergoing the structural transition from tetragonal to orthorhombic structure at 13 K, the experiment revealed a strong shift of the first magnetic excitation to higher energies [7]. Such a shift is qualitatively well reproduced by our first-principles electronic structure calculations despite a certain quantitative difference occuring between the experimental and calculated energy as discussed above. The experimentally observed development of the energy of the first excited CF level can thus be primarily ascribed to CF changes when transforming from tetragonal to orthorhombic structure.

Our calculations also show some clear changes of the phonon spectra when comparing the tetragonal and orthorhombic case. As far as the low-energy part of the of $CePd_2Al_2$ phonon spectra is concerned, there is a clear shift of the DOS (R+Pd atoms) to higher energies in the orthorhombic

structure with respect to the tetragonal structure. No such shift occurs for $LaPd_2Al_2$. This can point to different characteristics of the structural transition in $CePd_2Al_2$ and $LaPd_2Al_2$.

4. Conclusions

The first-principles electronic structure calculations for $CePd_2Al_2$ lead to crystal field excitations at 3.6 meV and 11.8 meV for the tetragonal structure and at 4.8 meV and 12.2 meV for the orthorhombic structure. The change for the first excited level agrees qualitatively well with the experiment. The energy of the second excited level fits perfectly with the model used to describe the inelastic neutron scattering data. We analyzed the mechanical properties based on the calculated elastic constants. Both phases of $LaPd_2Al_2$ and $CePd_2Al_2$ are of a ductile manner. The lattice dynamics calculations show that in both tetragonal and orthorhombic structures there are no imaginary modes for any q-wave vector within the Brillouin zone and therefore the lattice structures are stable. In addition, the zero point vibrations stabilize the orthorhombic structure with respect to the tetragonal one. There is a large phonon DOS at around 12 meV, i.e. at the same energy as the first excited state of the crystal field splitting and in agreement with the experimental observation [7]. The 4f electron-phonon coupling was not calculated because one cannot use the perturbation theory for $CePd_2Al_2$. Therefore, we can only suggest the existence of a bound CF state and phonons creating the vibron states, which was observed experimentally [7]. Furthermore, the calculation indicates a shift of the low frequency DOS (R + Pd atoms) to higher energies in the orthorhombic structure of $CePd_2Al_2$ with respect to the tetragonal structure. No such shift occurs for $LaPd_2Al_2$. The analysis by means of MSD, specific heat as well as estimation of the Debye temperature is also given.

Acknowledgment

This work was supported by the Czech Science Foundation under Grant No. 17-04925J. D L acknowledges support by the European Regional Development Fund in the IT4Innovations national supercomputing center—path to exascale project, project number CZ.02.1.01/0.0/0.0/16_013/0001791 within the Operational Programme Research, Development and Education and Mobility Grant No. 8J18DE004.

ORCID iDs

D Legut https://orcid.org/0000-0001-9185-9934

References

[1] Steglich F, Aarts J, Bredl C D, Lieke W, Meschede D, Franz W and Schäfer H 1979 *Phys. Rev. Lett.* **43** 1892–96
[2] Bellarbi B, Benoit A, Jaccard D, Mignot J M and Braun H F 1984 *Phys. Rev.* B **30** 1182
[3] Endstra T, Nieuwenhuys G J and Mydosh J A 1993 *Phys. Rev.* B **48** 9595
[4] Movshovich R, Graf T, Mandrus D, Thompson J D, Smith J L and Fisk Z 1996 *Phys. Rev.* B **53** 8241
[5] Jaccard D, Behnia K and Sierro J 1992 *Phys. Lett.* A **163** 475
[6] Chapon L C, Goremychkin E A, Osborn R, Rainford B D and Short S 2006 *Physica* B **819** 378–80
[7] Klicpera M, Boehm M, Doležal P, Mutka H, Koza M, Rols S, Adroja D T, Puente-Orench I, Rodriguez-Carvajal J and Javorský P 2017 *Phys. Rev.* B **95** 085107
[8] Loewenhaupt M, Rainford B D and Steglich F 1979 *Phys. Rev. Lett.* **42** 1709–12
[9] Loewenhaupt M, Reichardt W, Pynn R and Lindley E 1987 *J. Magn. Magn. Mater.* **63** 73–5
[10] Adroja D T, del Moral A, de la Fuente C, Fraile A, Goremychkin E A, Taylor J W, Hillier A D and Fernandez-Alonso F 2012 *Phys. Rev. Lett.* **108** 216402
[11] Thalmeier P and Fulde P 1982 *Phys. Rev. Lett.* **49** 1588
[12] Klicpera M, Javorský P and Hoser A 2014 *J. Alloys Compd.* **596** 167–72
[13] Klicpera M, Doležal P, Prokleška J, Prchal J and Javorský P 2015 *J. Alloys Compd.* **639** 51–9
[14] Tursina A, Khamitcaeva E, Gribanov A, Gnida D and Kaczorowski D 2015 *Inorg. Chem.* **54** 3439–45
[15] Beyermann W P, Hundley M F, Canfield P C, Godart C, Selsane M, Fisk Z, Smith J L and Thompson J D 1991 *Physica* B **171** 373
[16] Takabatake T, Tanaka T, Bando Y, Fujii H, Takeda N, Ishikawa M and Oguro I 1997 *Physica* B **230** 223–5
[17] Dommann A, Hullier F, Ott H R and Gramlich V 1985 *J. Less-Common Met.* **110** 331
[18] Kitagawa J and Ishikawa M 1999 *J. Phys. Soc. Japan* **68** 2380–3
[19] Doležal P, Klicpera M, Prchal J and Javorský P 2019 *J. Alloys Compd.* **790** 480–92
[20] Schwarz K, Blaha P and Madsen G 2002 *Comput. Phys. Commun.* **147** 71
[21] Perdew J P, Burke K and Ernzerhof M 1996 *Phys. Rev. Lett.* **77** 3865
[22] Diviš M, Rusz J, Michor H, Hilscher G, Blaha P and Schwarz K 2005 *J. Alloys Compd.* **403** 29
[23] Kresse G and Furthmüuller J 1996 *Phys. Rev.* B **54** 11169
[24] Kresse G and Furthmüuller J 1996 *Comput. Mater. Sci.* **6** 15
[25] Parlinski K, Li Z Q and Kawazoe Y 1997 *Phys. Rev. Lett.* **78** 4063
[26] Togo A, Chaput L, Tanaka I and Hug G 2010 *Phys. Rev.* B **81** 174301
[27] Novak P and Diviš M 2007 *Phys. Status Solidi* b **244** 3168
[28] Dove M T 1993 *Introduction to the Lattice Dynamics* (Cambridge: Cambridge University Press)
[29] Patrick Ch E and Staunton J B 2019 *J. Phys.: Condens. Matter* **31** 305901
[30] Wdowik U D and Legut D 2009 *J. Phys.: Condens. Matter* **21** 275402
[31] Klicpera M, Pásztorová J and Javorský P 2014 *Superconduc. Sci. Technol.* **27** 085001
[32] Wdowik U D and Parlinski K 2007 *Phys. Rev.* B **75** 104306
[33] Born M and Huang K 1954 *Dynamics Theory of Crystal Lattices* (Oxford: Oxford University Press)
[34] Mouhat F and Coudert F-X 2014 *Phys. Rev.* B **90** 224104
[35] Hill R 1952 *Proc. Phys. Soc.* A **65** 349
[36] Zhang S H and Zhang R F 2017 *Comput. Phys. Comm.* **220** 403
[37] Pugh S F 1954 *Phil. Mag.* **45** 823